The Effects of Projection Undersampling and Number of Projections on Aliasing Artifacts in Ultrasonic Tomographic Images in Air

I.J. O' Sullivan[1], W.M.D. Wright[2] and P. Ingleby[3]

Ultrasonics Research Group,
Department of Electrical and Electronic Engineering,
National University of Ireland - Cork,
IRELAND
E-mail: [1]ianos@rennes.ucc.ie, [2]bill.wright@ucc.ie, [3]pauli@rennes.ucc.ie

Abstract -- **A through-transmission fan-beam ultrasonic tomography system has been constructed to image solid objects and temperature fields in air. Image reconstruction has been achieved using a filtered backprojection algorithm combined with a re-bin routine and a difference technique. Aliasing artifacts, which arise in the reconstructed images due to projection undersampling, will be investigated and optimum sampling criteria for the minimisation of aliasing artifacts will be suggested.**

I INTRODUCTION

Computerised tomography is a method of reconstructing object images from projection data obtained by isonifying the object from many directions in the plane of interest [1]. The reconstructed image is a map of spatial variations in the acoustic properties of the object such as attenuation and slowness. These quantities can be directly related to such properties as temperature and density.

Images in computerised tomography may be reconstructed using transmission [2], diffraction [3] or reflection algorithms [4], depending upon the effect that the image field has upon the isonifying beam. Transmission tomography relies on the fact that ultrasound can pass through the area to be imaged without deflection. The application of transmission tomography principles in ultrasound has often proved inadequate due to the fact that the wavelength of the ultrasound is sometimes comparable to the size of the object being imaged, thus causing diffraction of the ultrasound beam. Transmission tomography algorithms, which account for such inhomogeneties have been reported by Mueller et al [5].

Images may be reconstructed in transmission tomography applications by using iterative or Fourier reconstruction techniques. Examples of iterative techniques such as ART and SIRT have been reported by Gordon et al [6] and Gilbert [7] respectively. Fourier methods such as Fourier inversion [8] and Filtered back projection [9] have been reported by Lewitt and Stark et al respectively.

In most process applications there are large variations in object homogeneity, which leads to invalid analysis when transmission tomography is applied, thus reflection or diffraction tomography methods must generally be employed. Transmission tomographic imaging in air [10,11] has been made possible in recent years due to improvements in electrostatic capacitance transducer manufacture and characterisation. These broadband transducers can generate and receive ultrasonic waves in air over a large frequency range and are ideal for accurate measurement of time of flight and frequency content.

A useful descriptor of the interaction of ultrasound with a material is its specific acoustic impedance, Z:

$$Z = \rho c \tag{1}$$

where ρ is the density of the material through which the ultrasound passes and c is the ultrasonic velocity through the material [12]. When considering the behaviour of an ultrasonic wavefront normal at an interface the power reflection coefficient, P_r is given in terms of the incident (p_i) and reflected (p_r) sound pressures [12]:

$$P_r = \left(\frac{p_r}{p_i}\right)^2 = \left[\frac{(Z_2 - Z_1)}{(Z_2 + Z_1)}\right]^2 \tag{2}$$

where Z_1 and Z_2 are the acoustic impedances of the two materials at the interface. It can therefore be shown that P_r for ultrasound passing from air at

300 K to air at 600 K is 0.111, and P_r for ultrasound passing from air at 300 K to aluminium is 0.999. It is clear that the greater the difference in impedance at the interface, the greater will be the amount of energy reflected, which is the case when a solid object is placed in an image field in air. Conversely, if the impedances are similar, for example regions of air at different temperatures, most of the energy is transmitted.

Transmission tomography of temperature fields using electrostatic transducers can thus be carried out effectively but when an object is placed in the image field, transmission projections will be incomplete due to reflection, and some of the ultrasound rays will be occluded. A modified version of the through transmission algorithm, which inserts artificial arrival times in place of the occluded waves will be implemented.

II THEORY

The local speed of sound is related to the propagation time t_{TR}, through a medium by the following relationship:

$$t_{TR} = \int_{r_T}^{r_R} \frac{dr}{c_r} \tag{3}$$

where c_r is the speed of sound at any position r along a sound ray path e.g. T_1 to R_1 (Figure 1). This integrand may also be referred to as the slowness [13].

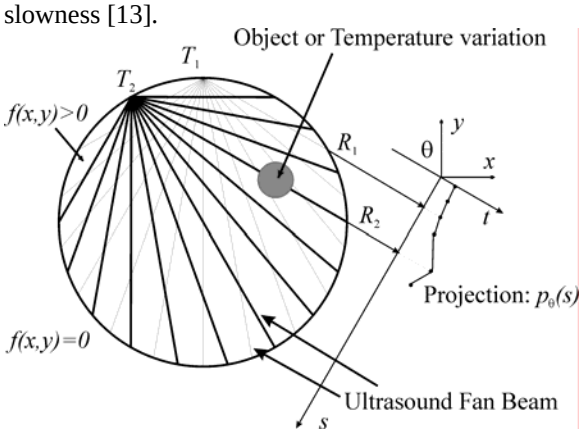

Figure 1: Fan Beam Geometry

The local speed of sound is also related to the temperature as follows:

$$c_r = 331.31\sqrt{\frac{T}{273.16}} \tag{4}$$

where T is the temperature of the air in Kelvin [14]. It has been shown that a reconstructed image of the spatial variation in slowness within the scanned area will indicate the presence of solid objects in air or changes in air temperature [11].

Using the capacitance electrostatic transducers it is possible to obtain through transmission data for the image field and images may be reconstructed using a modification of the filtered back projection for transmission tomography.

Figure 1 shows an image plane, which is uniformly interrogated from various viewpoints using ultrasound. The propagation time for a straight ultrasound ray (e.g. T_1 to R_1) in a projection at an angle θ to the *(x, y)* Cartesian axis equals a line integral of the slowness variation along its path, this may be represented as follows:

$$p_\theta(s) = \int_{-\infty}^{\infty} f_\theta(s,t)\,dt \tag{5}$$

where the function $p_\theta(s)$ represents the propagation times for an interrogation at an angle θ to the *(x, y)* Cartesian axis. The function $f_\theta(s,t)$ represents the slowness function along the ray path in the rotated *(s,t)* coordinates. The Fourier transform of this projection may be defined as:

$$P_\theta(S) = \int_{-\infty}^{\infty} p_\theta(s)e^{-j2\pi sS}\,ds \tag{6}$$

and inserting (5) into (6) gives:

$$P_\theta(S) = \int_{-\infty}^{\infty}\int_{-\infty}^{\infty} f_\theta(s,t)e^{-j2\pi sS}\,ds\,dt \tag{7}$$

The two dimensional transform of the slowness may be represented as follows:

$$F_\theta(S,T) = \int_{-\infty}^{\infty}\int_{-\infty}^{\infty} f_\theta(s,t)e^{-j2\pi(sS+tT)}\,ds\,dt \tag{8}$$

and when $T = 0$:

$$P_\theta(S) = F_\theta(S,0) = \int_{-\infty}^{\infty}\int_{-\infty}^{\infty} f_\theta(s,t)e^{-j2\pi sS}\,ds\,dt \tag{9}$$

Thus a one-dimensional Fourier transform of a projection at an angle θ is equal to the two-dimensional Fourier transform of the actual slowness function through the centre of the object at the same angle θ. When the non-rotated coordinates in the Fourier domain (X,Y) are considered it is clear that an inverse Fourier transform will provide an estimation of $f(x,y)$:

$$f(x,y) = \int_{-\infty}^{\infty} F(X,Y)e^{j2\pi(xX+yY)}\,dx\,dy \tag{10}$$

However the function $F(X,Y)$ is in polar coordinates in the Fourier domain and before an inverse Fourier transform can be attempted, the discrete data must be interpolated into Cartesian coordinates. This procedure can lead to large errors due to the fact that as the value of S increases the distance between sampling points becomes greater.

This problem may be overcome by converting the inverse Fourier transform expression into polar coordinates:

$$x = r\cos\phi \;,\; y = r\sin\phi \tag{11}$$

and:

$$X = R\cos\theta \;,\; Y = R\sin\theta \tag{12}$$

Rewriting (10) provides the following relationship:

$$f(x,y) = \int_0^{\pi}\int_{-\infty}^{\infty} F(R\cos\theta, R\sin\theta)e^{j2\pi(r\cos\phi R\cos\theta + r\sin\phi R\sin\theta)}|R|dRd\theta$$

$$f(x,y) = \int_0^{\pi} d\theta \int_{-\infty}^{\infty} F(R\cos\theta, R\sin\theta)e^{j2\pi rR\cos(\theta-\phi)}|R|dr \quad (13)$$

$|R|$ arises from the conversion of the differential area dXdY to polar coordinates as:

$$dXdY = |R|\, dRd\theta \quad (14)$$

and:

$$\cos\theta\cos\phi + \sin\theta\sin\phi = \cos(\theta - \phi) \quad (15)$$

Now from (9):

$$P_\theta(S) = F_\theta(S,T) = F(R\cos\theta, R\sin\theta) \quad (16)$$

therefore:

$$f(x = r\cos\phi, y = r\sin\phi) = \int_0^{\pi} d\theta \int_{-\infty}^{\infty} P_\theta |R| e^{j2\pi rR\cos(\theta-\phi)} dr \quad (17)$$

The product $P_\theta|R|$ in the Fourier domain may be represented by a convolution in the space domain, which may be represented as follows:

$$p_\theta * k(r) = g_\theta(r) \quad (18)$$

where $k(r)$ is known as a kernel function, which has a Fourier transform $|R|$. Equation (17) may be rewritten as:

$$f(x = r\cos\phi, y = r\sin\phi) = \int_0^{\pi} d\theta \int_{-\infty}^{\infty} G_\theta(R) e^{j2\pi rR\cos(\theta-\phi)} dr$$

where:

$$G_\theta = P_\theta|R| = \int_0^{\pi} g_\theta[r\cos(\theta-\phi)]d\theta \quad (19)$$

This represents a backprojection of all the convoluted projections $g_\theta[r\cos(\theta - \phi)]$ associated with all rays passing through a point (x,y).

If the convolution is performed in the space domain the algorithm may be termed convolution back projection and if the convolution is carried out in the Fourier domain the algorithm is known as the filtered back projection.

Practical applications using the above algorithm undoubtedly obtain discrete data therefore it is necessary to modify the algorithm to reconstruct images of slowness using discrete data. Assuming that m equiangular projections are sampled at n even intervals in steps of Δs, the frequency content of the convolutions will be bandlimited, with a bandwidth, B, determined according to the Nyquist sampling theorem;

$$B = \frac{1}{2\Delta s} \quad (20)$$

in order to reduce the effects of aliasing it is necessary to ensure that:

$$\Delta s = \frac{1}{2s_o} \quad (21)$$

where s_o is the highest spatial frequency of interest in the object. The Fourier representation of the ideal Kernel function $K(R) = |R|$ will tend to emphasize the higher frequencies, where the signal to noise ratio is worst. Applying a window function $W(R)$ reduces the effect of truncating the Kernel to zero above the cut off frequency, B. Zero padding to a length N such that N is a power of two and $N \geq (2n-1)$ reduces the problems caused by linear convolution. Taking all of these factors into account the following discrete data version of the filtered back projection algorithm may be presented:

$$G'_\theta(l\Delta R) = P_\theta(l\Delta R)|l\Delta R|W(l\Delta R) \quad (22)$$

$$= P_\theta(l\Delta R)K'_\theta(l\Delta R) \quad (23)$$

and:

$$g'_\theta(n\Delta r) \cong IFFT\{K'_\theta(l\Delta R).FFT(p_\theta(n\Delta r))\} \quad (24)$$

then:

$$f(k\Delta x, l\Delta y) \cong \Delta\theta \sum_m g'_{m\Delta\theta}(k\Delta x\cos\theta + l\Delta y\sin\theta) \quad (25)$$

where G'_θ, K'_θ and g'_θ are discrete representations of G_θ, K_θ and g_θ, respectively and l represents the effect of zero padding the data.

III SAMPLING GEOMETRY

A typical fan-beam sampling geometry employed is shown schematically in Figure 1. A source transducer T is positioned on the perimeter of a circular area of interest and a receiver R is scanned through a number of regularly spaced positions opposite the source to produce a fan shaped series of ultrasonic waves known as a projection. This procedure is then repeated at different source positions T_1, T_2, etc until a series of projections is obtained.

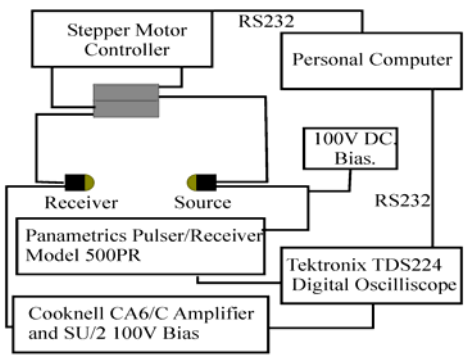

Figure 2: Tomographic Rig.

Once the fan beam projections have been obtained, the rays must be re-binned in order to produce a data set of equally spaced parallel rays at each projection angle. The re-bin routine firstly rescales all rays to an equal length using the first ray in each fan beam projection as a reference. It is assumed that the first ray in each projection passes through the extremity of the scan area and is not influenced by any disturbances within the scan area. It may thus be used to calculate a value ofbackground reference velocity. All parallel rays at each projection angle are subsequently extracted and as they are unequally spaced an interpolation routine is implemented in order to create a data set of equally spaced parallel rays.

IV EXPERIMENTAL SETUP

In order to create the fan beam isonification of the image plane as shown in Figure 1 it is necessary to employ a divergent ultrasonic source receiver. The experimental configuration is shown schematically in Figure 2. Ultrasound was generated and received by a pair of prototype electrostatic transducers with convex polished metal backplates, a 10mm radius of curvature and 5 μm metalized Mylar film. These devices operated at a frequency of 400 kHz with a –6 dB bandwidth of 300 kHz, whose basic operation has been detailed elsewhere [15].

The transmitters were driven by a Panametrics Pulser/Receiver (Model 500PR) providing a -250V pulse with a pulse energy of up to 19.4 μJ. A Cooknell CA6/C charge amplifier with a sensitivity of 250 mV amplified each received signal, which was then digitized and displayed on a Tektronix TDS 224 oscilloscope before being transferred to a PC via a RS232 interface for storage and analysis. All transducers had an applied dc bias voltage of +100V. The transducers were mounted on Daedal rotary stages driven using stepper motors and custom electronics under RS232 control to an accuracy of 0.02°. The image plane was scanned at 5° intervals from 72 source transducer locations over 360°. Each individual source scan fan beam was evenly sampled at 2.5° intervals, from 37 receiver positions opposite the source, in a 90° arc centred

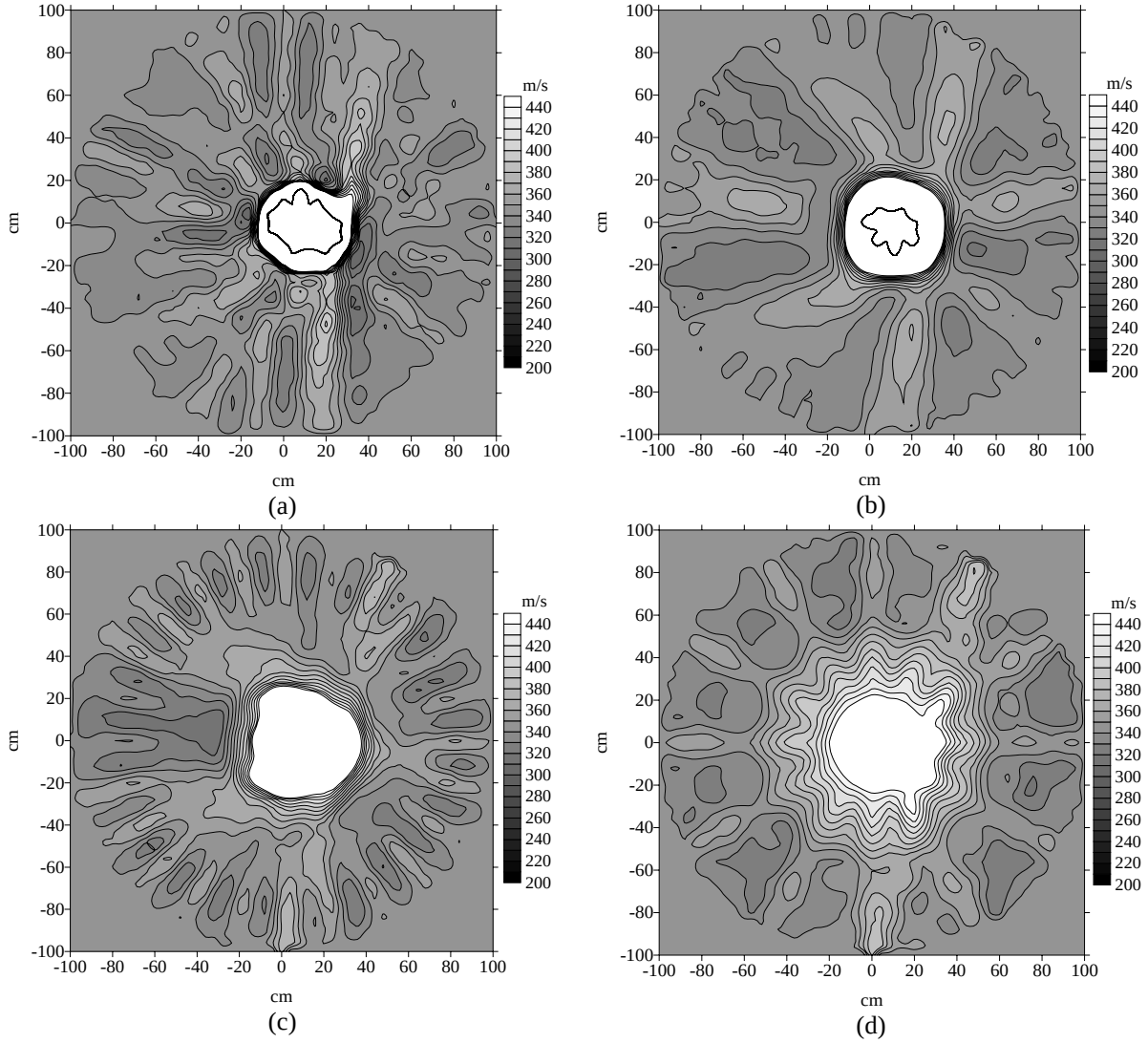

Figure 3: Reconstructions of a 38mm aluminium bar using (a) 2664 rays, (b) 684 rays, (c) 312 rays and (d) 84 rays

along the diameter of the scan. The data acquisition and transducer movement was carried out under computer control via a RS232 serial interface.

V RESULTS & DISCUSSION

Reconstructions of object images and temperature fields using fan beam tomography can be seen in Figure 3(a) to (d) and Figure 4(a) to (d) respectively. Figures 3(a) and 4 (a) were reconstructed using a full set of experimental scan data which consists of 2664 time-of-flight measurements (rays). Figures 3(b) and 4(b) were reconstructed using a reduced data set, representing an experimental set-up of 36 source transducers and 19 receiver transducers with an angular separation of 5° (684 rays). Figures 3(c) and 4(c) represent 24 transmitters and 13 receivers with an angular separation of 7.5° (312 rays) and finally Figures 3(d) and 4(d) represent 12 transmitters and 7 receivers with an angular separation of 15° (84 rays).

Figure 3(a) accurately reconstructs the position and the diameter of a 38mm aluminium bar located 10mm to the right of centre of the image plane, however as the number of projections (and samples) decreases the algorithm has increased difficulty in reproducing the objects size and shape. To avoid aliasing when attempting to reconstruct an object of diameter 38mm, a spatial sampling rate of at least 52.63 m^{-1} is required. Figure 3(a) and (b) are sampled at a rate of 122.7 m^{-1} and 60.25 m^{-1} respectively. Figure 3(b) shows no obvious aliasing effects. This image has been reconstructed using about one quarter of the original data, which corresponds to a considerable time saving during data acquisition. Figure 3(c) shows evidence of aliasing with distinct streaks linking the centre of the scan area to the transducer positions creating a star shaped pattern. This type of aliasing artifact is also known as Gibbs phenomenon [1]. The sampling rate in this case is 39.76 m^{-1}. Figure 3(d) shows aliasing to a greater extent due to an even lower sampling rate of 19.23 m^{-1}.

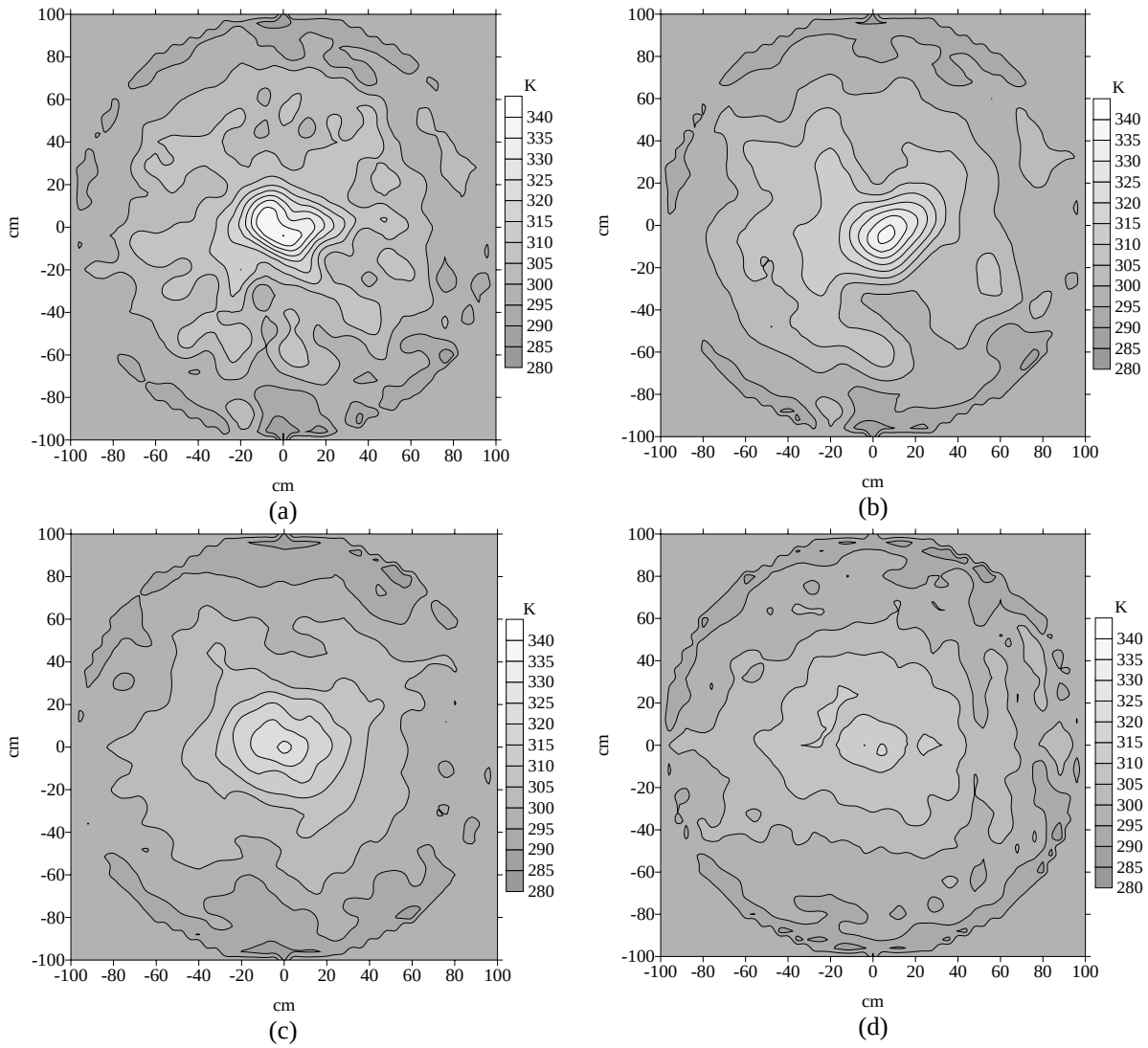

Figure 4: Reconstructions of a temperature field using (a) 2664 rays, (b) 684 rays, (c) 312 rays and (d) 84 rays

Figure 4 shows the reconstruction of a temperature field in air 40 mm above a 573 K heat source of diameter 4 mm, using the same sampling rates and source/receiver arrangements as Figure 3. The effect of aliasing in these images is not as obvious and all reconstructions reproduce the background temperature of 299 K. A K-type thermocouple and a Digitron 2000T thermometer were used to measure the temperature directly above the heat source in the scanning plane and a value of 344 K was obtained. Figures 4(a) and (b) reconstruct centre temperatures of 340 K and 337 K respectively. These temperatures equate to accuracies of 98.8% and 97.9% respectively.

It is clear from Figure 4(a) that the area of increased temperature has a diameter of approximately 40 mm (equating to a minimum sampling rate of approximately 50 m^{-1}). As was the case with the object imaging the reconstruction in Figure 4(b) again gives an accurate reconstruction when only one quarter of the original data is utilised. Figures 4(c) and (d) reconstruct centre temperatures of 326 K and 315 K respectively, which equate to accuracies of 94.8% and 91.6% respectively. This drop off in accuracy can again be attributed to aliasing effects resulting from sampling rates below 50 m^{-1}.

VI CONCLUSIONS

Tomographic reconstructions of object and temperature fields of approximate diameter 40 mm, within a scan area of diameter 100mm, using various sampling geometries have been carried out in air using prototype electrostatic transducers. The object images (Figure 3) show reconstructions of the diameter and the position of the aluminium bar with decreasing resolution as the number of projections (and samples) was reduced. The temperature images (Figure 4) all reconstruct the background velocity but the values of centre temperature are shown to diminish with accuracies of 99.8%, 97.9%, 94.8% and 91.6% when the number of rays utilised was 2664, 684, 312 and 84 rays respectively.

Reducing the data set by 75% (684 rays) produced no appreciable loss in accuracy in the solid object reconstruction, but any further reduction in the number of projections and samples was associated with the introduction of aliasing artifacts. However in this work the temperature images do not exhibit the expected Gibbs phenomena but the effects of reducing the sampling rate can clearly be seen in the accuracy of the centre temperature reconstruction.

VII REFERENCES

[1] A.C. Kak and M.Slaney, Principles of computerized tomography, IEEE Press, New York, 1988.

[2] A.M.H. Satti and J. Szilard, "Computerized ultrasonic tomography for testing solid propellant rocket motors", *Ultrasonics*, Volume 21, 162-166, 1983.

[3] L. Capineri, H.G. Tattersall, J.A.G. Temple and M.G. Silk, "Time of flight diffraction tomography for NDT applications"*Ultrasonics*, Volume 30, 275-288, 1992.

[4] K.A. Dines and S.A. Goss, "Computed Ultrasonic Reflection Tomography" ", *IEEE Transactions on Ultrasonics, Ferroelectrics and Frequency Control*, Volume 34, 309-318, 1987.

[5] R.K. Mueller, M. Kaveh and G. Wade, "Reconstructive tomography and applications to ultrasonics", *Proc. IEEE*, Volume 69, 567-587, 1979.

[6] R. Gordon, R. Bender and G.T. Herman, "Algebraic reconstruction techniques for three dimensional electron microscopy and X-Ray photography", *Journal of Theoretical Biology*, Volume 29, 471-481, 1970.

[7] P. Gilbert, "Iterative methods for the three dimensional reconstruction of an object from projections" *Journal of Theoretical Biology*, Volume 31, 105-117, 1972.

[8] R.M. Lewitt, "Reconstruction Algorithms: transform methods" *Proc. IEEE*, Volume 71, 390-408, 1984.

[9] H.H Stark, J.W. Wood, I. Paul and R. Hingorani, "Direct Fourier Reconstruction in computer tomography", *IEEE Transactions on Acoustics, Speech and Signal Processing*, Volume 29, 237-245, 1981.

[10] W.M.D. Wright, D.A. Hutchins, D.P. Jansen and D.W. Schindel, "Air-Coupled Lamb Wave Tomography", *IEEE Transactions on Ultrasonics, Ferroelectrics and Frequency Control*, Volume 44, No 1, 53-59, January 1997.

[11] W.M.D. Wright, D.W. Schindel, D.A. Hutchins, P.W. Carpenter and D.P. Jansen, "Ultrasonic Tomographic imaging of temperature and flow fields in gases using air –coupled capacitance transducers", *Journal of the Acoustical Society of America*, Vol 104, No 6, 3446-3455, 1998.

[12] R.A. Williams, M.S. Beck, Process Tomography; Principles, techniques and applications. Butterworth & Heinemann Publishers, London, 1995.

[13] K.B. Winters and D. Rouseff, "Tomographic reconstruction of stratified fluid flow", *IEEE Transactions on Ultrasonics, Ferroelectrics and Frequency Control*, Vol ume 40, 26-33, 1993.

[14] R. Hickling and S.P. Martin, "The use of ultrasound for gauging and proximity sensing in air", *Journal of the Acoustical Society of America*, Volume 79, 1151-1160, 1986.

[15] D.W. Schindel, D.A. Hutchins, L. Zou and .M. Sayer, " The Design and Characterisation of Micromachined Air-Coupled Capacitance Transducers", *IEEE Transactions on Ultrasonics, Ferroelectrics and Frequency Control*, Volume 42, No 1, 1995.